International Journal of Engineering Science 49 (2011) 589–605

Contents lists available at ScienceDirect

International Journal of Engineering Science

journal homepage: www.elsevier.com/locate/ijengsci

Analytical and numerical analysis of 3D grid-reinforced orthotropic composite structures

E.M. Hassan [a], A.V. Georgiades [b,*], M.A. Savi [c], A.L. Kalamkarov [a]

[a] Department of Mechanical Engineering, Dalhousie University, Halifax, Nova Scotia, B3J 2X4, Canada
[b] Department of Mechanical Engineering and Materials Science and Engineering, Cyprus University of Technology, Limassol, Cyprus
[c] Department of Mechanical Engineering, COPPE, Universidade Federal do Rio de Janeiro, Rio de Janeiro, RJ, Brazil

ARTICLE INFO

Article history:
Received 20 October 2010
Received in revised form 26 January 2011
Accepted 17 February 2011
Available online 12 March 2011

Keywords:
Asymptotic homogenization method
Finite element method
3D grid-reinforced orthotropic composite structures
Effective elastic coefficients

ABSTRACT

A comprehensive micromechanical investigation of 3D periodic composite structures reinforced with a grid of orthotropic reinforcements is undertaken. Two different modeling techniques are presented; one is based on the asymptotic homogenization method and the other is a numerical model based on the finite element technique. The asymptotic homogenization model transforms the original boundary value problem into a simpler one characterized by effective coefficients which are shown to depend only on the geometric and material parameters of a periodicity cell. The model is applied to various 3D grid-reinforced structures with generally orthotropic constituent materials. Analytical formula for the effective elastic coefficients are derived, and it is shown that they converge to earlier published results in much simpler case of 2D grid reinforced structures with isotropic constituent materials. A finite element model is subsequently developed and used to examine the aforementioned periodic grid-reinforced orthotropic structures. The deformations from the finite element simulations are used to extract the elastic and shear moduli of the structures. The results of the asymptotic homogenization analysis are compared to those pertaining to their finite element counterparts and a very good agreement is shown between these two approaches. A comparison of the two modeling techniques readily reveals that the asymptotic homogenization model is appreciably faster in its implementation (without a significant loss of accuracy) and thus is readily amenable to preliminary design of a given 3D grid-reinforced composite structure. The finite element model however, is more accurate and predicts all of the effective elastic coefficients. Thus, the engineer facing a particular design application, could perform a preliminary design (selection of type, number and spatial orientation of the reinforcements) and then fine tune the final structure by using the finite element model.

1. Introduction

Recent years have witnessed a considerable increase in the science and technology of fiber reinforced composite materials due to their wide-ranging engineering applications. They are successfully utilized in a variety of applications where high strength, enhanced stiffness, low weight, excellent durability and design flexibility are required. Examples of modern applications where one encounters advanced composites include reinforcement, retrofitting and structural health-monitoring components in the civil and structural engineering industries, (Kalamkarov, Fitzgerald, MacDonald, & Georgiades (1999,

* Corresponding author. Tel.: +357 2500 2560; fax: +357 2500 2769.
E-mail address: tasos.georgiades@cut.ac.cy (A.V. Georgiades).

0020-7225/$ - see front matter © 2011 Elsevier Ltd. All rights reserved.
doi:10.1016/j.ijengsci.2011.02.004

2000)), aerospace, automotive and marine engineering components of all sizes, medical prosthetic devices, sports and recreational goods and others. Larger-scale incorporation and further exploitation of composite materials for novel applications will undoubtedly be facilitated if their macroscopic behavior can be predicted at the design stage. Accordingly, comprehensive micromechanical models must be developed.

Partial differential equations describing the behavior of most composite materials are characterized by the presence of rapidly varying coefficients due to the presence of numerous embedded inclusions in close proximity to one another. To treat these equations analytically, one, therefore, has to consider two sets of spatial variables, one for the microscopic characteristics of the constituents and the other for the macroscopic behavior of the composite under investigation. The presence of the microscopic and macroscopic scales in the original problem frequently renders the pertinent partial differential equations extremely difficult to solve. Clearly, the ensuing analysis would be significantly simplified if the two scales could be decoupled and each one handled separately. For a practically important type of regular composite structures one technique that permits us to accomplish precisely this is the asymptotic homogenization method. The basic outcome of asymptotic homogenization is to essentially "even out" substructural fluctuations that inevitably characterize an inhomogeneous periodic structure due to the property mismatch of the different constituents and yield a homogenized structure with averaged or effective properties that are homogeneous from one point to the next within the periodicity cell. Once determined, the effective coefficients are universal in nature and can be used, in lieu of the actual material coefficients, to both analyze a wide variety of structures under numerous loading conditions, and design a composite with desirable properties, specifically tailored towards a particular engineering application. The mathematical framework of asymptotic homogenization can be found in Bensoussan, Lions, and Papanicolaou (1978), Sanchez-Palencia (1980), Bakhvalov and Panasenko (1984), and Cioranescu and Donato (1999). The asymptotic homogenization method has been used to analyze periodic composite and smart structures, see e.g. the pioneering work by Duvaut (1976) on inhomogeneous plates. Other work can be found in Caillerie's heat conduction studies pertaining to thin elastic and periodic plates (Caillerie, 1984), Kohn and Vogelius (1984, 1985) who used asymptotic homogenization to analyze the pure bending of a linearly elastic homogeneous plate with rapidly varying thickness, and Kalamkarov (1992) who examined a wide variety of elasticity and thermoelasticity problems pertaining to composite materials and thin-walled composite structures reinforced shells and plates. Kalamkarov and Kolpakov (2001) dealt with the piezoelastic problem of a 3D thin composite solid and calculated the effective elastic and piezoelectric coefficients of the homogenized structure. Kalamkarov and Georgiades (2002a, 2002b)] derived expressions for the effective elastic, piezoelectric and hygrothermal expansion coefficients for general 3D periodic smart composite structures. The same authors (Kalamkarov & Georgiades, 2004; Georgiades & Kalamkarov, 2004) developed comprehensive asymptotic homogenization models for smart composite plates with rapidly varying thickness and periodically arranged actuators. These models were subsequently used to determine general expressions for the effective coefficients of the homogenized plates and the work was illustrated by means of different examples such as constant-thickness laminates and wafer- and rib-reinforced smart composite plates; Georgiades, Challagulla, and Kalamkarov (2006) applied a general 3D micromechanical model for thin smart composite plates reinforced with a network of cylindrical reinforcements that may also exhibit piezoelectric behavior. Challagulla, Georgiades, and Kalamkarov (2007) developed a comprehensive 3D asymptotic homogenization model pertaining for anisotropic periodic composite structures reinforced with a spatial network of isotropic reinforcements. Challagulla, Georgiades, and Kalamkarov (2010) Georgiades, Challagulla, and Kalamkarov (2010) developed asymptotic homogenization models for thin network-reinforced smart composite shells. Other work can be found in Andrianov, Danishevs'kyy, and Kalamkarov (2006), Kalamkarov, Andrianov, and Danishevs'kyy (2009, 2006), Saha, Kalamkarov, and Georgiades (2007a, 2007b).

Since the work of Suquet (1987), a considerable number of micromechanically oriented numerical approaches based on the finite element method have been developed and extensively used in the analysis of the mechanical properties of composite materials with spatial repetition of a small microstructure. Adams and Crane (1984) developed a 2D finite element approach for a microscopic region of a unidirectional composite using a generalized plane strain formulation which includes longitudinal shear loading. The method of cells (Aboudi, 1989) and its generalization (Paley & Aboudi, 1992) have proven to be particularly successful micromechanical analysis tools for the prediction of the overall behavior of various types of composites with known properties and geometrical arrangement of the individual constituents and give consistently accurate results for the elastic properties. Both theories (Aboudi, 1989; Paley & Aboudi, 1992), discretize the material microstructure using rectangular subcells and assume linear expansions for the displacement field within the subcells. A review of the work conducted using the two theories has been given by Aboudi (1996). Guedes and Kikuchi (1990) studied the numerical accuracy of the finite element method when computing the homogenized material properties of a composite material and presented a numerical technique to predict such properties by using microscale holes subjected to tractions based on the asymptotic expansion of the deformation field. Bennett and Haberman (1996) presented an alternative approach that retains the philosophy of Aboudi's Method of Cells. The equations of equilibrium are applied to a representative volume element and a unified method of homogenization of micromechanical effects is presented. The finite element method has been extensively used to examine unit cell problems and to determine the effective properties and damage mechanisms of composites. The applications considered include unidirectional laminates (Allen & Boyd, 1993), cross-ply laminates (Bigelow, 1993), woven and braided textile composites (Bystrom, Jekabsons, & Varna, 2000; Dasgupta, Agarwal, & Bhandarkar, 1996; Tan, Tong, & Steven, 1997; Wang, Wang, Zhou, & Zhou, 2007) and many others.

Pertaining to the various finite element models, the unit cells employed can be subjected to mechanical, thermal, electrical or other loading types. The introduction of the loading conditions to the representative unit cell is expressed, in general,

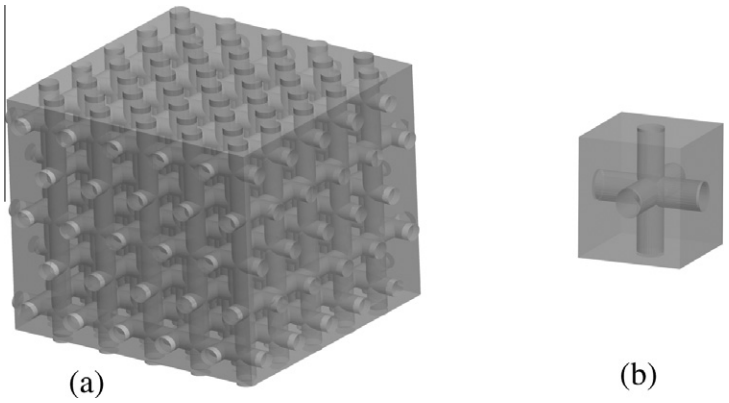

Fig. 1. (a) Cubic grid-reinforced structure with reinforcements in y_1, y_2, y_3 directions and (b) its unit cell.

in terms of macroscopic or averaged field quantities, such as stress or strain. Li (1999) and Li and Wongsto (2004) studied the use of the unit cells of different shapes (square, hexagonal etc.) for the analysis and modeling of unidirectional fiber reinforced composites, by considering the symmetries in the material and deriving appropriate periodic boundary conditions for the unit cell. The loads on the unit cell and its response in terms of macroscopic stresses or strains have been addressed in such a way that the effective properties of the material can be obtained from the micromechanical analysis of the unit cell in a standard manner. In the study of Sun and Vaidya (1996) appropriate boundary conditions used to model various loading conditions are determined by judicious use of symmetry and periodicity conditions.

The work of Pettermann and Suresh (2000) involved piezoelectric composites and employed a rigorous finite element unit cell model to account for local fluctuations of the fields. A full set of material moduli, i.e. the macroscopic elastic, dielectric and piezoelectric coefficients were determined. The concept of 'macroscopic degrees of freedom' and the implementation of periodicity conditions for composites with periodic microstructure composed of linear or nonlinear constituents were discussed in Michel, Moulinec, and Suquet (1999). The two commonly used boundary conditions in micromechanics are uniform tractions and uniform displacements. Sluis, Schreurs, Brekelmans, and Meijer (2000) investigated applicability of both types of boundary conditions on a plate with a regular square array of inclusions. Miehe, Schroder, and Bayreuther (2002) applied a numerical procedure for the computation of the overall macroscopic elasticity moduli of linear composite materials with periodic micro-structure. The underlying key approach is a finite element discretization of the boundary value problem for the fluctuation field on the micro-structure of the composite. A number of possible unit cell models can be developed according to the material microstructure. Recently, Xia, Zhang, and Ellyin (2003) developed a 3D unit cell model for both unidirectional and cross ply laminates. The proposed unified boundary conditions satisfy not only the boundary displacement periodicity but also the boundary traction periodicity of the representative volume element model. A FEM-based micromechanical analysis of unidirectional periodic piezoelectric cylindrical fiber composites subjected to different loading conditions with different boundary conditions to predict the effective coefficients of transversely isotropic piezoelectric cylindrical fiber (1–3 connectivity) composites is proposed by Berger et al. (2006). The study of Oliveira, Pinho-da-Cruz, and Teixeira-Dias (2009) has integrated the asymptotic homogenization method into a finite element simulation to derive overall material properties for metal matrix composites reinforced with spherical ceramic particles.

The main purpose of the present work is to provide an in-depth micromechanical modeling of 3D grid-reinforced composite structures such as the one depicted in Fig. 1. In the present study it is assumed that the constitutive materials are generally orthotropic and this makes it much more complicated than the previously published results limited to the isotropic constitutive materials.

Following this introduction, the rest of the paper is organized as follows: The basic problem formulation and the general asymptotic homogenization model for 3D grid-reinforced composite structures is derived in Section 2. Section 3 illustrates the applicability of the model with the help of specific examples. Section 4 discusses the development of the finite element model and Section 5 formulates and compares results of both, analytical and numerical approaches via different examples of varying complexity. Finally, Section 6 concludes the work.

2. Asymptotic homogenization model for three-dimensional structures

2.1. General model

Consider a general composite structure representing an inhomogeneous solid occupying domain Ω with boundary $\partial\Omega$ that contains a large number of periodically arranged reinforcements as shown in Fig. 2(a). It can be observed that this structure is obtained by repeating a small unit cell Y with boundary Γ within the domain Ω, see Fig. 2(b).

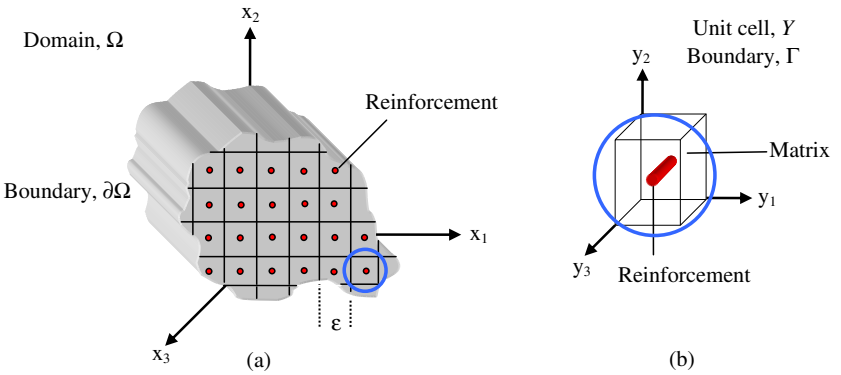

Fig. 2. (a) Three-dimensional periodic composite structure, (b) unit cell *Y*.

The elastic deformation of this structure can be described by means of the following boundary-value problem:

$$\frac{\partial \sigma_{ij}^{\varepsilon}}{\partial x_j} = f_i \text{ in } \Omega \quad \text{with } u_i^{\varepsilon}(x) = 0 \text{ on } \partial\Omega \tag{1}$$

where,

$$\sigma_{ij}^{\varepsilon}\left(x, \frac{x}{\varepsilon}\right) = C_{ijkl}\left(\frac{x}{\varepsilon}\right) e_{kl}^{\varepsilon}\left(x, \frac{x}{\varepsilon}\right) \tag{2a}$$

$$e_{ij}^{\varepsilon}\left(x, \frac{x}{\varepsilon}\right) = \frac{1}{2}\left[\frac{\partial u_i}{\partial x_j}\left(x, \frac{x}{\varepsilon}\right) + \frac{\partial u_j}{\partial x_i}\left(x, \frac{x}{\varepsilon}\right)\right] \tag{2b}$$

Here and in the sequel, all indices assume values of 1, 2 and 3, and the summation convention is adopted. C_{ijkl} is the tensor of elastic coefficients, e_{kl} is the strain tensor which is a function of the displacement field u_i, and, finally, f_i represent body forces. It is assumed in Eq. (2a) that the C_{ijkl} coefficients are all periodic with a unit cell Y of characteristic dimension ε. Small parameter ε is made non-dimensional by dividing the size of the unit cell by a certain characteristic dimension of the overall structure. Consequently, the periodic composite structure of Fig. 2 is seen to be made up of a large number of unit cells periodically arranged within the domain Ω. It is noteworthy to mention at this point that if the boundary conditions in second term of Eq. (1) were made non-zero to examine a very general model, then boundary-layer type solutions will result (see Kalamkarov & Georgiades (2002b)). However, the obtained effective coefficients will not change.

2.2. Asymptotic expansions, governing equations, and unit cell problems

The development of the general asymptotic homogenization model pertaining to the 3D smart composite structures and grid-reinforced smart composites can be found in Kalamkarov and Georgiades (2002a, 2002b) and Hassan et al. (2009). In this section only a brief overview will be given in so far as the main results will be used in subsequent sections of the paper. The first step is to define the so-called "fast" or microscopic variables according to:

$$y_i = \frac{x_i}{\varepsilon} \tag{3}$$

As a consequence, the boundary value problem and corresponding stress field defined in Eqs. (1) and (2a) become:

$$\frac{\partial \sigma_{ij}^{\varepsilon}}{x_j} + \frac{1}{\varepsilon}\frac{\partial \sigma_{ij}^{\varepsilon}}{\partial y_j} = f_i \text{ in } \Omega \quad \text{with } u_i^{\varepsilon}(\mathbf{x}, \mathbf{y}) = 0 \text{ on } \partial\Omega \tag{4}$$

$$\sigma_{ij}^{\varepsilon}(\mathbf{x}, \mathbf{y}) = C_{ijkl}(y)\frac{\partial u_k}{\partial x_l}(\mathbf{x}, \mathbf{y}) \tag{5}$$

The next step is to consider asymptotic expansions for the displacement and stress fields in terms of the small parameter ε:

$$u^{\varepsilon}(\mathbf{x}, \mathbf{y}) = u^{(0)}(\mathbf{x}, \mathbf{y}) + \varepsilon u^{(1)}(\mathbf{x}, \mathbf{y}) + \varepsilon^2 u^{(2)}(\mathbf{x}, \mathbf{y}) + \cdots \tag{6a}$$

$$\sigma_{ij}^{\varepsilon}(\mathbf{x}, \mathbf{y}) = \sigma_{ij}^{(0)}(\mathbf{x}, \mathbf{y}) + \varepsilon\sigma_{ij}^{(1)}(\mathbf{x}, \mathbf{y}) + \varepsilon^2\sigma_{ij}^{(2)}(x, y) + \cdots \tag{6b}$$

It is understood that all functions in $\boldsymbol{y}$ are periodic with the unit cell Y as shown in Eq. (2b). By substituting (6b) into (4) and considering terms with like powers of ε one obtains a series of differential equations involving sequential terms of the stress field expansion, see Kalamkarov & Georgiades (2002a). The first two of these are:

$$\frac{\partial \sigma_{ij}^{(0)}}{\partial y_j} = 0 \quad and \quad \frac{\partial \sigma_{ij}^{(0)}}{\partial x_j} + \frac{\partial \sigma_{ij}^{(1)}}{\partial y_j} = f_i \tag{7}$$

where

$$\sigma_{ij}^{(0)} = C_{ijkl}\left(\frac{\partial u_k^{(0)}}{\partial x_l} + \frac{\partial u_k^{(1)}}{\partial y_l}\right) \quad and \quad \sigma_{ij}^{(1)} = C_{ijkl}\left(\frac{\partial u_k^{(1)}}{\partial x_l} + \frac{\partial u_k^{(2)}}{\partial y_l}\right) \tag{8}$$

Combination of the first expressions in Eqs. (7) and (8) leads to the following expression:

$$\frac{\partial}{\partial y_j}\left(C_{ijkl}\frac{\partial u_k^{(1)}(\mathbf{x},\mathbf{y})}{\partial y_l}\right) = -\frac{\partial C_{ijkl}(y)}{\partial y_j}\frac{\partial u_k^{(0)}(x)}{\partial x_l} \tag{9}$$

The separation of variables on the right-hand-side of Eq. (9) prompts us to write down the solution for $\mathbf{u}^{(1)}$ as:

$$u_m^{(1)}(\boldsymbol{x},\boldsymbol{y}) = \frac{\partial u_k^{(0)}(\boldsymbol{x})}{\partial x_l} N_m^{kl}(\boldsymbol{y}) \tag{10}$$

where functions N_m^{kl} are periodic in y and satisfy

$$\frac{\partial}{\partial y_j}\left(C_{ijmn}(y)\frac{\partial N_m^{kl}(\boldsymbol{y})}{\partial y_n}\right) = -\frac{\partial C_{ijkl}}{\partial y_j} \tag{11}$$

One observes that Eq. (11) depends entirely on the fast variable $\boldsymbol{y}$ and is thus solved on the domain Y of the unit cell, remembering at the same time that both C_{ijkl} and N_m^{kl} are Y-periodic in $\boldsymbol{y}$. Consequently, Eq. (11) is appropriately referred to as the *unit-cell problem*. The next important step in the model development is the homogenization procedure. This is carried out by first substituting (10) into (8), and integrating the resulting expression over the domain Y of the unit cell (with volume $|Y|$) remembering to treat x_i as a parameter as far as integration with respect to y_j is concerned. This yields,

$$\widetilde{C}_{ijkl}\frac{\partial^2 u_k^{(0)}(\boldsymbol{x})}{\partial x_j \partial x_l} = f_i \tag{12}$$

where the following definition is introduced:

$$\widetilde{C}_{ijkl} = \frac{1}{|Y|}\int_Y \left(C_{ijkl}(\boldsymbol{y}) + C_{ijmn}(\boldsymbol{y})\frac{\partial N_m^{kl}}{\partial y_n}\right) dv \tag{13}$$

The coefficients $\widetilde{C}_{ijkl}$ denote the homogenized or effective elastic coefficients. It is noticed that these effective coefficients are free from the inhomogeneity complications that characterize their actual rapidly varying material counterparts, C_{ijkl}, and as such, are more amenable to analytical and numerical treatment. The effective coefficients shown above are universal in nature and can be used to study a wide variety of boundary value problems associated with a given composite structure. Once determined, any dependency on the fast variable $\boldsymbol{y}$ is removed and consequently Eq. (12) which represents the "homogenized problem", contains terms that are functions solely of the slow variables $\boldsymbol{x}$.

2.3. Three-dimensional grid-reinforced composites

In the sequel, we will consider the problem of a general macroscopically anisotropic 3D composite structure reinforced with N families of reinforcements, see for instance Fig. 1 where an explicit case of 3 families of reinforcements is shown. We assume the members of each family are made of dissimilar, generally orthotropic materials and have relative orientation angles $\theta_1^n,\ \theta_2^n,\ \theta_3^n$ (where $n = 1,2,\ldots,N$) with the y_1, y_2, y_3 axes, respectively. It is further assumed that the orthotropic reinforcements have significantly higher elasticity moduli than the matrix material, so we are justified in neglecting the contribution of the matrix phase in the analytical treatment. Clearly, for the particular case of framework or lattice network structures the surrounding matrix is absent and this is modeled by assuming zero matrix rigidity. The nature of the network structure of Fig. 1 is such that it would be more efficient if we first considered a simpler type of unit cell made of only a single reinforcement as shown in Fig. 3. Having solved this, the effective elastic coefficients of more general structures with several families of reinforcements can be readily determined by the superposition of the solution for each of them found separately. In following this procedure, one must naturally accept the error incurred at the regions of intersection between the reinforcements. However, our approximation will be quite accurate because these regions of intersection are highly localized and do not contribute significantly to the integral over the entire unit cell domain. A complete mathematical justification for this argument in the form of the so-called principle of the split homogenized operator has been provided by Bakhvalov & Panasenko (1984). In order to calculate the effective coefficients of the simpler structure of Fig. 3, unit cell problem given by Eq. (11) must be solved and, subsequently, Eq. (13) must be applied.

The problem formulation for the structure shown in Fig. 3 begins with the introduction of the following notation, see Hassan, Kalamkarov, Georgiades, & Challagulla (2009):

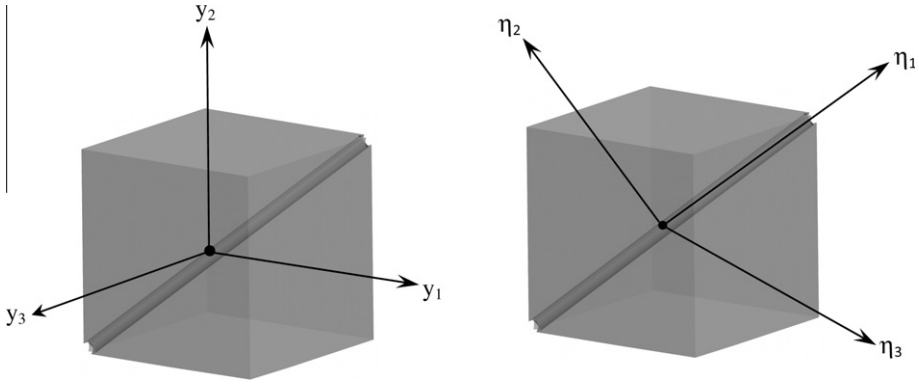

Fig. 3. Unit cell (single reinforcement family) in original and rotated microscopic coordinates.

$$b_{ij}^{kl} = C_{ijmn}(\boldsymbol{y})\frac{\partial N_m^{kl}(y)}{\partial y_n} + C_{ijkl} \tag{14}$$

With this definition in mind the unit cell of the problem given by Eq. (11) is solved as:

$$b_{mm}^{mm} = C_{mmmm} + \begin{bmatrix} \lambda_1^{mm}\{C_{m1}q_{21} + C_{m6}q_{22} + C_{m5}q_{23}\} + \lambda_2^{mm}\{C_{m1}q_{31} + C_{m6}q_{32} + C_{m5}q_{33}\} + \\ \lambda_3^{mm}\{C_{m6}q_{21} + C_{m2}q_{22} + C_{m4}q_{23}\} + \lambda_4^{mm}\{C_{m6}q_{31} + C_{m2}q_{32} + C_{m4}q_{33}\} + \\ \lambda_5^{mm}\{C_{m5}q_{21} + C_{m4}q_{22} + C_{m3}q_{23}\} + \lambda_6^{mm}\{C_{m5}q_{31} + C_{m4}q_{32} + C_{m3}q_{33}\} \end{bmatrix} \tag{15a}$$

$$b_{mn}^{mn} = C_{mnmn} + \begin{bmatrix} \lambda_1^{mn}\{C_{mn11}q_{21} + C_{mn12}q_{22} + C_{mn13}q_{23}\} + \lambda_2^{mn}\{C_{mn11}q_{31} + C_{mn12}q_{32} + C_{mn13}q_{33}\} + \\ \lambda_3^{mm}\{C_{mn12}q_{21} + C_{mn22}q_{22} + C_{mn23}q_{23}\} + \lambda_4^{mn}\{C_{mn12}q_{31} + C_{mn22}q_{32} + C_{mn23}q_{33}\} + \\ \lambda_5^{mm}\{C_{mn13}q_{21} + C_{mn22}q_{21} + C_{mn33}q_{23}\} + \lambda_6^{mm}\{C_{mn13}q_{31} + C_{mn23}q_{32} + C_{mn33}q_{33}\} \end{bmatrix} \tag{15b}$$

where there is no summation on either index "m" or "n". As well, q_{ij} represent the components of the matrix of the direction cosines characterizing the axes rotation in Fig. 3. The constants λ_i^{kl} in Eq. (15a) satisfy the following linear algebraic equations:

$$\begin{aligned} &A_1\lambda_1^{kl} + A_2\lambda_2^{kl} + A_3\lambda_3^{kl} + A_4\lambda_4^{kl} + A_5\lambda_5^{kl} + A_6\lambda_6^{kl} + A_7^{kl} = 0 \\ &A_8\lambda_1^{kl} + A_9\lambda_2^{kl} + A_{10}\lambda_3^{kl} + A_{11}\lambda_4^{kl} + A_{12}\lambda_5^{kl} + A_{13}\lambda_6^{kl} + A_{14}^{kl} = 0 \\ &A_{15}\lambda_1^{kl} + A_{16}\lambda_2^{kl} + A_{17}\lambda_3^{kl} + A_{18}\lambda_4^{kl} + A_{19}\lambda_5^{kl} + A_{20}\lambda_6^{kl} + A_{21}^{kl} = 0 \\ &A_{22}\lambda_1^{kl} + A_{23}\lambda_2^{kl} + A_{24}\lambda_3^{kl} + A_{25}\lambda_4^{kl} + A_{26}\lambda_5^{kl} + A_{27}\lambda_6^{kl} + A_{28}^{kl} = 0 \\ &A_{29}\lambda_1^{kl} + A_{30}\lambda_2^{kl} + A_{31}\lambda_3^{kl} + A_{32}\lambda_4^{kl} + A_{33}\lambda_5^{kl} + A_{34}\lambda_6^{kl} + A_{35}^{kl} = 0 \\ &A_{36}\lambda_1^{kl} + A_{37}\lambda_2^{kl} + A_{38}\lambda_3^{kl} + A_{39}\lambda_4^{kl} + A_{40}\lambda_5^{kl} + A_{41}\lambda_6^{kl} + A_{42}^{kl} = 0 \end{aligned} \tag{16}$$

Here, A_i^{kl} are constants which depend on the geometric parameters of the unit cell and the material properties of the reinforcement. The explicit expressions for these constants are given in Hassan et al. (2009). Once the system in Eq. (16) is solved, the determined λ_i^{kl} coefficients are substituted back into Eqs. (15a) and (15b) to obtain the b_{ij}^{kl} coefficients. In turn, these are used to calculate the effective elastic coefficients of the 3D grid-reinforced by integrating over the volume of the unit cell as it will be explained below.

2.4. Effective elastic coefficients

The effective elastic moduli of the 3D grid-reinforced composite with generally orthotropic reinforcements with a unit cell shown in Fig. 3 are obtained on the basis of Eq. (13), which, on account of notation (14) becomes:

$$\widetilde{C}_{ijkl} = \frac{1}{|Y|}\int_Y b_{ij}^{kl}dv \tag{17}$$

Noting that b_{ij}^{kl} are constants, and denoting the length and cross-sectional area of the reinforcement (in coordinates y_1, y_2, y_3) by L and A respectively, and the volume of the unit cell by V, the effective elastic coefiicients become

$$\widetilde{C}_{ijkl} = \frac{AL}{V}\cdot b_{ij}^{kl} = V_f \cdot b_{ij}^{kl} \tag{18}$$

where V_f is the volume fraction of the reinforcement within the unit cell. For structures with more than one family of reinforcements (a particular case of which is shown in Fig. 1) the effective moduli can be obtained by superimposition, see Hassan et al. (2009).

One observes, that on the basis of the developed asymptotic homogenization model and Eqs. (17) and (18), the rapidly varying elastic coefficients (which fluctuate significantly over a microscopic length scale of order ε as one moves from one constituent, such as the matrix, to another, such as a reinforcement) of the original composite structure are replaced by homogeneous effective coefficients which are, understandably, much more amenable to analysis and design. These effective coefficients can be used to analyse a broad range of structural applications and, importantly, can be used to efficiently and expediently design and optimize a composite structure to conform to a particular engineering application.

3. Examples of 3D grid-reinforced composite structures

The developed micromechanical model and methodology presented in this work can be applied to the analysis and design of a wide range of practically important types of 3D grid-reinforced composite structures with orthotropic reinforcements. Let us consider as an illustrative example the case of the simple 3D grid reinforced structure shown in Fig. 1. This structure has three families of generally orthotropic reinforcements, each family oriented along one of the coordinate axes, as shown in Fig. 1. Noting that in this case $q_{ij} = \delta_{ij}$, where δ_{ij} is the Kronecker Delta, the values of λ_i^{kl} for the reinforcement in the y_1 direction are obtained from Eq. (16) and then substituted into (15a) and (15b) to determine the local functions b_{ij}^{kl} for orthotropic reinforcements. Subsequently, one substitutes expressions for the elastic coefficients to obtain:

$$b_{11}^{11} = E_1^{(1)}, \quad b_{11}^{22} = b_{11}^{33} = b_{11}^{23} = b_{11}^{13} = b_{11}^{12} = 0, \quad b_{22}^{kl} = b_{33}^{kl} = b_{23}^{kl} = b_{13}^{kl} = b_{12}^{kl} = 0 \tag{19}$$

Here, $E_1^{(1)}$ is the principal Young's modulus of the reinforcement oriented in the y_1 direction. Repeating the procedure for the reinforcement in the y_2 direction yields $b_{22}^{22} = E_1^{(2)}$ with the remaining coefficients equal to zero, and for the reinforcement in the y_3 direction the only non-zero coefficient is $b_{33}^{33} = E_1^{(3)}$.

We are now in a position to calculate the effective elastic coefficients of the cubic grid structures of Fig. 1. We denote the length (within the unit cell) and cross-sectional area of the i-th reinforcement in the y_i direction by L_i and A_i respectively (in coordinates y_1, y_2, y_3) and the principal Young's modulus of that reinforcement by $E_1^{(i)}$. Then, for a unit cell of volume V, the corresponding volume fraction γ_i is given by $\gamma_i = A_i L_i / V$. Therefore, the non-vanishing effective elastic coefficients for the composite grid-reinforced structure of Fig. 1 are:

$$\widetilde{C}_{11} = \gamma_1 \cdot E_1^{(1)}; \quad \widetilde{C}_{22} = \gamma_2 \cdot E_1^{(2)}; \quad \widetilde{C}_{33} = \gamma_3 \cdot E_1^{(3)} \tag{20}$$

It is observed that all the off-diagonal terms in the effective stiffness matrix are zero. This is partly because the reinforcements in a particular direction have no effect on the stiffness of the structure in the directions perpendicular to it and partly due to the fact that the matrix stiffness is neglected in this model. As expected, increasing the volume fraction of any or all of the reinforcements will increase the stiffness of the composite in the three principal directions.

Let us now consider a 2D analogue of the structure of Fig. 1, by assuming that the reinforcements whereby the reinforcements lie entirely in the y_1–y_2 plane and let us assume that the reinforcements are isotropic. Then, the effective coefficients for a unit cell with a single reinforcement oriented at an angle θ with the y_1 axis calculated on the basis of the derived model are:

$$\begin{aligned} &\widetilde{C}_{11} = \tfrac{AL}{V} \cdot E \cdot \cos^4\theta, \quad \widetilde{C}_{22} = \tfrac{AL}{V} \cdot E \cdot \sin^4\theta, \quad \widetilde{C}_{12} = \widetilde{C}_{66} = \tfrac{AL}{V} \cdot E \cdot \cos^2\theta \sin^2\theta, \\ &\widetilde{C}_{16} = \tfrac{AL}{V} \cdot E \cdot \cos^3\theta \sin\theta, \quad \widetilde{C}_{26} = \tfrac{AL}{V} \cdot E \cdot \cos\theta \sin^3\theta, \quad \textit{with} \quad \widetilde{C}_{ij} = \widetilde{C}_{ji} \end{aligned} \tag{21}$$

These results are identical to those obtained earlier by Kalamkarov (1992), who used asymptotic homogenization techniques, and by Pshenichnov (1982), who used a different approach based on stress–strain relationships in the reinforcements.

If we further consider a simpler case comprising of a single reinforcement oriented in, say, the y_3 direction, our model predicts the value of the effective Young's Modulus E_3 to be γE_f where E_f is the stiffness of the reinforcement. The results predicted by our model agree well with relevant results from earlier work by Pobedrya (1984), and Mol'kov & Pobedrya (1985) as well as numerical results by Kalamkarov, Kudryavtsev, & Parton (1987) and experimental results, see for example Maksimov, Plume, & Ponomarev (1983). For example, for organic plastic fibers oriented along the y_3 direction (and having a stiffness of 127.5 GPa in the y_3 direction and volume fraction of 48%) embedded in soft isotropic matrix with stiffness 3.236 GPa, the effective Young's Modulus predicted by our model is 61.2 MPa. The corresponding numerical value predicted by Kalamkarov et al. (1987) was 62.6 MPa and the average experimental value predicted by Maksimov et al. (1983) was 62.8 MPa.

Let us now consider a more interesting 3D composite structure shown in Fig. 4. As seen from the unit cell of the structure in Fig. 5, three reinforcements are oriented along the main diagonals and the fourth spans from the middle of the lower rear edge to the middle of the top front edge.

One proceeds by first solving for the λ_i^{kl} coefficients from Eq. (16) and subsequently obtains the b_{ij}^{kl} functions from Eqs. (15a) and (15b). The effective coefficients are then readily obtained from Eq. (18). The resulting analytical expressions are too lengthy to be reproduced here; however, typical effective elastic coefficients are plotted in Figs. 6 and 7. For the purposes of these figures, it is assumed that the reinforcements are made of carbon with material properties given in Table 1.

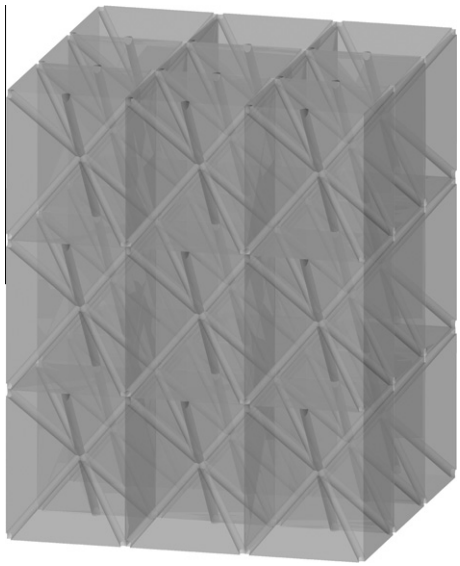

Fig. 4. Composite grid structure with diagonally oriented generally orthotropic reinforcements.

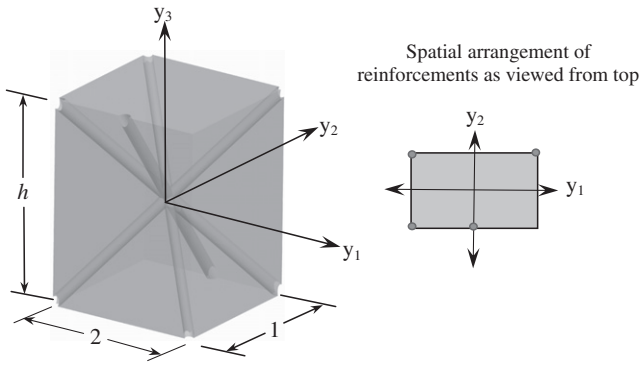

Fig. 5. Unit cell of the composite grid structure of Fig. 4.

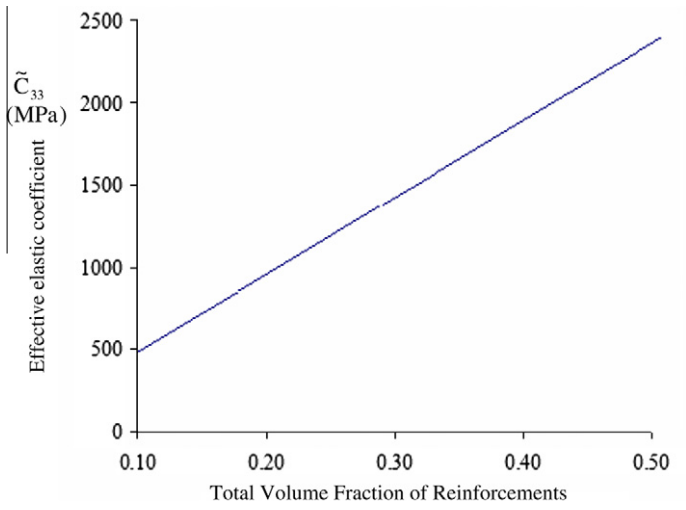

Fig. 6. Plot of $\tilde{C}_{33}$ effective coefficient vs. total reinforcement volume fraction for the composite grid structure shown in Figs. 4 and 5.

Table 1
Material properties of orthotropic carbon reinforcements (Reddy, 2004).

E_1	E_2	E_3	G_{12}	G_{13}	G_{23}	v_{12}	v_{13}	v_{23}
Reinforcement material properties								
173.0 Gpa	33.1 GPa	5.2 GPa	9.4 GPa	8.3 GPa	3.2 GPa	0.036	0.25	0.171

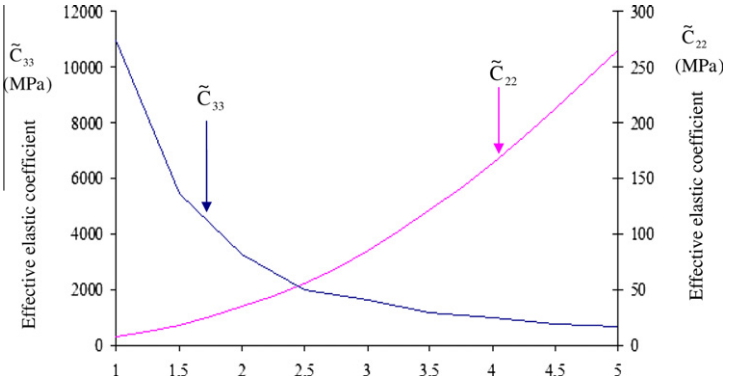

Fig. 7. Plot of the effective coefficient $\tilde{C}_{22}$ and $\tilde{C}_{33}$ vs. relative height of the unit cell for structure S_2.

Fig. 6 shows a plot of a typical effective coefficient, $\tilde{C}_{33}$, for the composite structure of Figs. 4 and 5. As expected, increasing the volume fraction of the reinforcements increases the value of all effective coefficients. A more interesting plot which highlights the versatility of the model and its propensity for design of 3D grid-reinforced composites is shown in Fig. 7. Fig. 7 represents a plot of $\tilde{C}_{22}$ and $\tilde{C}_{33}$ vs. the relative height of the unit cell. The relative height of the unit cell is simply the ratio of the height to the length of the unit cell (with the width kept constant).

The cross-sectional area of the reinforcements is increased progressively to maintain a constant total reinforcement volume fraction as the overall volume of the unit cell is increased. We note that increasing the relative height of the unit cell forces the reinforcements to be oriented progressively closer to the y_3 axis, and, correspondingly, further away from the y_1 and y_2 axes. As a consequence, we anticipate an increase in the stiffness in the y_3 direction and a corresponding decrease in the stiffness in the y_2 direction. Fig. 7 shows precisely that.

What is important to realize however is that these trends can easily be changed by modifying various material or geometric parameters. For instance, had we kept the diameter of the reinforcements constant in this example we would be facing two competing effects when increasing the height of the unit cell; an increase in the degree of inclination of the reinforcements to the y_3 direction (which increases $\tilde{C}_{33}$) and a corresponding decrease in the volume fraction of the reinforcements (which reduces $\tilde{C}_{33}$). Thus, the overall variation of $\tilde{C}_{33}$ would be different than the one shown in Fig. 7. In other words, the developed model is completely general in that it affords the designer flexibility in selecting different material and geometrical parameters of interest to design a composite with desirable effective properties so as to conform to a particular engineering application.

4. Numerical micromechanical modeling using finite element method

The finite element model presented in this study is based on examining a representative element of the material, equivalent to the unit cell. It takes into account all pertinent parameters such as geometric, material and loading. The results are compared with corresponding results of the asymptotic homogenization analysis as developed in the above part of the paper.

The developed finite element approach consists of three basic steps. It begins with the determination and prescription of appropriate periodic boundary conditions to the representative unit cell. Subsequently, the non-homogenous strain fields obtained from the analysis are reduced to volume averaged strain, and finally, the effective elastic coefficients of the pertinent composite structure are obtained as a ratio of the average stress to the average strain. The average stresses and strains in the unit cell are defined by

$$\tilde{\sigma}_{ij} = \frac{1}{V}\int_V \sigma_{ij} dV \tag{22a}$$

$$\tilde{\varepsilon}_{ij} = \frac{1}{V}\int_V \varepsilon_{ij} dV \tag{22b}$$

where V is the volume of the periodic unit cell, and σ_{ij} and ε_{ij} are local (microscopic) stresses and strains in the unit cell. The average strain $\tilde{\varepsilon}_{ij}$ can be related to the periodic boundary displacements of the unit cell by means of the divergence theorem (Lai, Rubin, & Krempl, 1993) as follows:

$$\tilde{\varepsilon}_{ij} = \frac{1}{V}\int_V \varepsilon_{ij} dV = \frac{1}{2V}\int_S (u_i n_j + u_j n_i) dS \tag{23}$$

where V and S are, respectively, the volume and boundary surface of the unit cell, u_i is the displacement and n_j the unit normal to S.

4.1. Unit cell model

To investigate the applicability of the finite element method in determining the effective elastic coefficients of grid-reinforced orthotropic composite structures various geometries have been analyzed. We will consider consequently a 2D grid-reinforced structure, a simple 3D model with three mutually orthogonal reinforcements oriented along the three coordinate axes, and, finally, a 3D structure with a rhombic arrangement of orthotropic reinforcements: two reinforcements are oriented in the y_1–y_2 plane at 45° to one another with a third reinforcement oriented along the y_3 axis. These structures are referred to in the sequel as structures A_1, A_2 and A_3 respectively and are shown in Figs. 8–10.

4.2. Periodic boundary conditions

The first step in the determination of the effective coefficients is the application of periodic boundary conditions to the unit cell. In this work a continuity displacement condition has been selected and prescribed to the boundaries of the unit cell in terms of periodic displacement boundary conditions. Hence, opposite surfaces of the unit cell are constrained to have equivalent deformation.

The periodical boundary conditions must be applied on the boundary Γ of the unit cell model shown in Fig. 2(b) to ensure that there is no separation or overlap between the neighboring unit cells.

According to Suquet (1987), the displacement field for a periodically arranged structure can be expressed as:

$$u_i = \tilde{\varepsilon}_{ij} y_j + u_i^*, \tag{24}$$

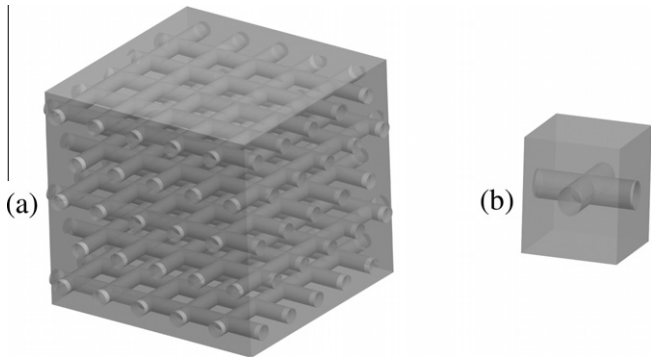

Fig. 8. (a) 2D Composite structure, A_1, with reinforcements oriented along y_1 and y_2 directions. (b) A representative unit cell.

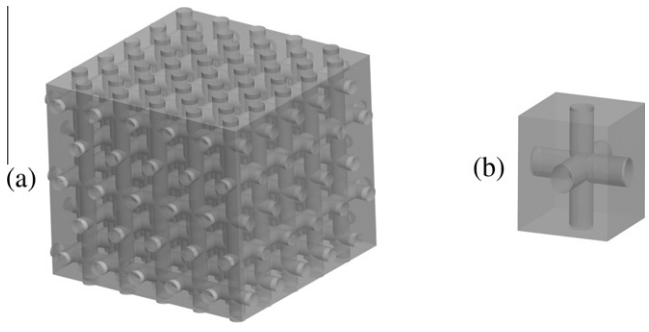

Fig. 9. (a) 3D Composite structure, A_2, with reinforcements oriented along y_1, y_2 and y_3 directions. (b) A representative unit cell.

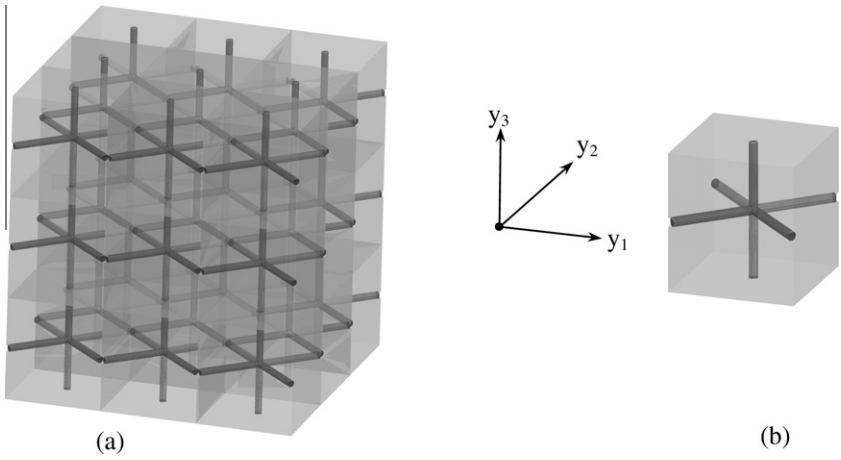

Fig. 10. (a) 3D Grid-reinforced composite structure, A_3, with reinforcements arranged in a rhombic fashion. (b) A representative unit cell.

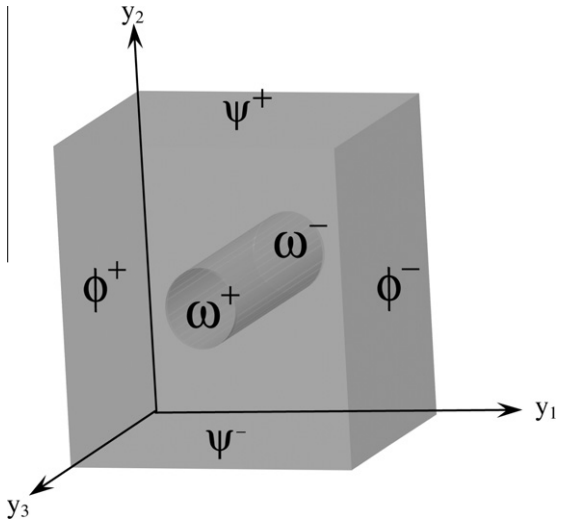

Fig. 11. Schematic diagram of the unit cell with notation of surfaces.

where $\tilde{\varepsilon}_{ij}$ indicates the macroscopic (global or average) strains of the unit cell, u_i^* is periodic function in (y_1,y_2,y_3), and y_j is the Cartesian coordinate of a unit cell point. The term $\tilde{\varepsilon}_{ij}y_j$ represents a linearly distributed displacement field while the term u_i^* accounts for the periodicity from one unit cell to another. The periodic term u_i^* represents a modification of the linear displacement field due to the presence of the inhomogeneous inclusions.

The equations describing the displacement fields on different boundary surfaces of the unit cell, see Fig. 11, are summarized as follows:

$$\begin{aligned} u_i^{\phi+} &= \tilde{\varepsilon}_{ij}y_j^{\phi+} + u_i^*; \quad u_i^{\phi-} = \tilde{\varepsilon}_{ij}y_j^{\phi-} + u_i^* \\ u_i^{\psi+} &= \tilde{\varepsilon}_{ij}y_j^{\psi+} + u_i^*; \quad u_i^{\psi-} = \tilde{\varepsilon}_{ij}y_j^{\psi-} + u_i^* \\ u_i^{\omega+} &= \tilde{\varepsilon}_{ij}y_j^{\omega+} + u_i^*; \quad u_i^{\omega-} = \tilde{\varepsilon}_{ij}y_j^{\omega-} + u_i^* \end{aligned} \tag{25}$$

It should be noted that the periodicity function $u_i^*(y_1,y_2,y_3)$ is identical at the two opposite boundaries. The boundary conditions (25) can be applied in the finite element model in form of the nodal displacement constraint equations.

The convergence of the finite element modeling has been analyzed to determine a reasonable balance between accuracy and computing time. A perfect bonding at the fiber matrix interface was assumed and various models of increasingly finer discretization were developed to determine whether results have converged satisfactorily. In all models denser meshes were created at the boundaries of the unit cells and around the interface, particularly for models with a larger reinforcement volume fraction. A mesh density of a representative unit cell (structure A_2) is shown in Fig. 12. For this model, mesh

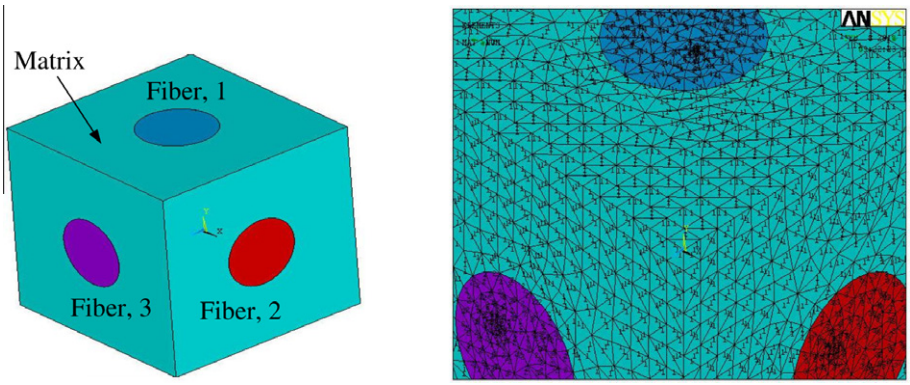

Fig. 12. 3D discretized meshing of unit cell model of structure A_2.

convergence was attained for approximately 63,000 elements. Similar mesh convergence studies were performed for all models presented in this paper.

4.3. Constitutive relations

The most general stress–strain relationship for an orthotropic material presented in indicial notation in Eq. (2a) can be expressed in matrix form as follows:

$$\begin{bmatrix} \tilde{\sigma}_{11} \\ \tilde{\sigma}_{22} \\ \tilde{\sigma}_{33} \\ \tilde{\sigma}_{23} \\ \tilde{\sigma}_{13} \\ \tilde{\sigma}_{12} \end{bmatrix} = \begin{bmatrix} \widetilde{C}_{11} & \widetilde{C}_{12} & \widetilde{C}_{13} & 0 & 0 & 0 \\ \widetilde{C}_{12} & \widetilde{C}_{22} & \widetilde{C}_{23} & 0 & 0 & 0 \\ \widetilde{C}_{13} & \widetilde{C}_{23} & \widetilde{C}_{33} & 0 & 0 & 0 \\ 0 & 0 & 0 & \widetilde{C}_{44} & 0 & 0 \\ 0 & 0 & 0 & 0 & \widetilde{C}_{55} & 0 \\ 0 & 0 & 0 & 0 & 0 & \widetilde{C}_{66} \end{bmatrix} \begin{bmatrix} \tilde{\varepsilon}_{11} \\ \tilde{\varepsilon}_{22} \\ \tilde{\varepsilon}_{33} \\ \tilde{\varepsilon}_{23} \\ \tilde{\varepsilon}_{13} \\ \tilde{\varepsilon}_{12} \end{bmatrix} \tag{26a}$$

$$\begin{bmatrix} \tilde{\varepsilon}_{11} \\ \tilde{\varepsilon}_{22} \\ \tilde{\varepsilon}_{33} \\ \tilde{\varepsilon}_{23} \\ \tilde{\varepsilon}_{13} \\ \tilde{\varepsilon}_{12} \end{bmatrix} = \begin{bmatrix} \widetilde{S}_{11} & \widetilde{S}_{12} & \widetilde{S}_{13} & 0 & 0 & 0 \\ \widetilde{S}_{12} & \widetilde{S}_{22} & \widetilde{S}_{23} & 0 & 0 & 0 \\ \widetilde{S}_{13} & \widetilde{S}_{23} & \widetilde{S}_{33} & 0 & 0 & 0 \\ 0 & 0 & 0 & \widetilde{S}_{44} & 0 & 0 \\ 0 & 0 & 0 & 0 & \widetilde{S}_{55} & 0 \\ 0 & 0 & 0 & 0 & 0 & \widetilde{S}_{66} \end{bmatrix} \begin{bmatrix} \tilde{\sigma}_{11} \\ \tilde{\sigma}_{22} \\ \tilde{\sigma}_{33} \\ \tilde{\sigma}_{23} \\ \tilde{\sigma}_{13} \\ \tilde{\sigma}_{12} \end{bmatrix} \tag{26b}$$

Here $\widetilde{C}_{ij}$ and $\widetilde{S}_{ij}$ denote the effective elastic stiffnesses and compliances while $\tilde{\sigma}_{ij}$ and $\tilde{\varepsilon}_{ij}$ denote average values of stress and strain. In the above matrices, the original composite structure is replaced by its effective homogenized counterpart. It is usually more convenient to express this constitutive relation in terms of the familiar engineering constants, see e.g. (Daniel & Ishai, 2006):

$$\begin{bmatrix} \tilde{\varepsilon}_{11} \\ \tilde{\varepsilon}_{22} \\ \tilde{\varepsilon}_{33} \\ \tilde{\varepsilon}_{23} \\ \tilde{\varepsilon}_{13} \\ \tilde{\varepsilon}_{12} \end{bmatrix} = \begin{bmatrix} \frac{1}{\widetilde{E}_1} & -\frac{\tilde{\nu}_{21}}{\widetilde{E}_2} & -\frac{\tilde{\nu}_{31}}{\widetilde{E}_3} & 0 & 0 & 0 \\ -\frac{\tilde{\nu}_{12}}{\widetilde{E}_1} & \frac{1}{\widetilde{E}_2} & -\frac{\tilde{\nu}_{32}}{\widetilde{E}_3} & 0 & 0 & 0 \\ -\frac{\tilde{\nu}_{13}}{\widetilde{E}_1} & -\frac{\tilde{\nu}_{23}}{\widetilde{E}_2} & \frac{1}{\widetilde{E}_3} & 0 & 0 & 0 \\ 0 & 0 & 0 & \frac{1}{\widetilde{G}_{23}} & 0 & 0 \\ 0 & 0 & 0 & 0 & \frac{1}{\widetilde{G}_{13}} & 0 \\ 0 & 0 & 0 & 0 & 0 & \frac{1}{\widetilde{G}_{12}} \end{bmatrix} = \begin{bmatrix} \tilde{\sigma}_{11} \\ \tilde{\sigma}_{22} \\ \tilde{\sigma}_{33} \\ \tilde{\sigma}_{23} \\ \tilde{\sigma}_{13} \\ \tilde{\sigma}_{12} \end{bmatrix} \tag{27}$$

The $\widetilde{C}_{ij}$ coefficients are calculated using the asymptotic homogenization method and then the corresponding compliance matrix $\widetilde{S}_{ij}$ is found by inverting the stiffness matrix; in turn the effective engineering constants of the homogenized composite structure are calculated from Eqs. (26a), (26b) and (27). In the present analysis, the reinforcement material is considered to be elastic and orthotropic while the matrix material is considered to be elastic and isotropic.

5. Results and discussion

We now compare results of the analytical (asymptotic homogenization) and numerical (finite element) models for the various examples of 3D grid-reinforced structures. The reinforcement material properties used in this study are given in the Table 1, and the matrix material properties are given in the Table 2.

In the subsections below, the representative effective elastic coefficients are determined and compared with respect to the unit cell spatial arrangement and the volume fraction of the reinforcements.

5.1. Calculation of the effective coefficients using the finite element method

In order to calculate the effective elastic coefficient $\widetilde{E}_1$, the appropriate constraint equations must be imposed on the ϕ^+ surface (see Fig. 11) with the average or macroscopic strain $\tilde{\varepsilon}_{11}$ in the y_1 direction as non-zero (while all other mechanical strains applied to the remaining faces of the unit cell, ϕ^-, ψ^+/ψ^-, ω^+/ω^-, are set to zero). This is achieved via the application of the appropriate constraining expressions in (25) to yield:

$$\begin{aligned} u_1^{\phi+} - u_1^{\phi-} &= \tilde{\varepsilon}_{11}(y_1^{\phi+} - y_1^{\phi-}) \\ u_2^{\psi+} - u_1^{\psi-} &= \tilde{\varepsilon}_{22}(y_1^{\psi+} - y_1^{\psi-}) = 0 \\ u_3^{\omega+} - u_3^{\omega-} &= \tilde{\varepsilon}_{33}(y_1^{\omega+} - y_1^{\omega-}) = 0 \end{aligned} \tag{28}$$

Since a zero displacement is applied to the ϕ^- surface in the y_1 direction the periodic boundary condition in (28) becomes:

$$u_1^{\phi+} = \tilde{\varepsilon}_{11}(y_1^{\phi+} - y_1^{\phi-}) \tag{29}$$

If, for the sake of convenience and without loss of generality, the edge length of the representative unit cell is taken as unity, then:

$$y_1^{\phi+} - y_1^{\phi-} = 1 \tag{30}$$

It should be noted that via the divergence theorem in (23) the macroscopic strain $\tilde{\varepsilon}_{11}$ in the y_1 direction can be related to the imposed boundary displacement in the same direction. Using Eq. (22a) the average value of stress $\tilde{\sigma}_{11}$ can be calculated and accordingly $\tilde{E}_1$ is determined from the constitutive matrix (27).

Similar procedure is applied to calculate $\widetilde{E}_2$ and $\widetilde{E}_3$.

Calculation of the effective shear moduli also proceeds in a similar manner. Thus, to calculate $\widetilde{G}_{12}$ we use the following constraint equations:

$$\begin{aligned} &u_1^{\psi+} - u_1^{\psi-} = 0; \quad u_2^{\phi+} - u_2^{\phi-} = \tilde{\varepsilon}_{12}; \quad u_3^{\omega+} - u_3^{\omega-} = 0; \\ &u_1^{\psi+} - u_1^{\psi-} = \tilde{\varepsilon}_{21}; \quad u_2^{\omega+} - u_2^{\omega-} = 0; \quad u_3^{\phi+} - u_3^{\phi-} = 0; \end{aligned} \tag{31}$$

From Eq. (27) $\widetilde{G}_{12}$ is obtained from the ratio $\tilde{\sigma}_{12}/\tilde{\varepsilon}_{12}$. Similar procedure is applied to calculate $\widetilde{G}_{13}$ and $\widetilde{G}_{23}$.

5.2. Comparison of the analytical and numerical results

We will consequently consider the 3D grid-reinforced structures A_1, A_2 and A_3, shown in Figs. 8–10.

5.2.1. Structure A_1

First we will consider structure A_1 shown in Fig. 8 with the constituent material properties given in Tables 1 and 2. Fig. 13 shows a variation of the effective elastic coefficient $\widetilde{E}_1$ (equal to $\widetilde{E}_3$) vs. the total reinforcement volume fraction. Three different lines are shown in this figure. The first line represents the asymptotic homogenization (AHM) results, the second line represents the finite element (FEM) results only considering the reinforcement contribution (i.e. neglecting the matrix), and the last line represents the FEM results which include both the reinforcement and matrix contributions.

Certain interesting observations are apparent from the Fig. 13. First of all the high degree of conformity between the first and second lines (they are practically indistinguishable) validate the accuracy of the asymptotic homogenization model in the case when the matrix contribution is neglected. We recall that in the derivation of the model in Section 3 we assumed that the reinforcements were much stiffer than the matrix and we consequently neglected the contribution of the latter. The discrepancy between the first and third lines is due to the contribution of the matrix. Fig. 13 also validates another key assumption of the asymptotic homogenization model. In particular, in Section 3 we noted that in using superposition to

Table 2
Material properties of isotropic epoxy matrix (Mallick, 2007).

E	ν
Matrix material properties	
3.6 GPa	0.35

determine the effective properties of structures with two or more families of reinforcements, an error will be incurred at the region of overlap between the reinforcements. However, we assumed that for the practical purposes this error will not contribute significantly to the integral in Eq. (17) and thus will not appreciably affect the effective coefficients. This assumption is confirmed by the excellent agreement between the first and second lines in Fig. 13. Of course, we expect that in more

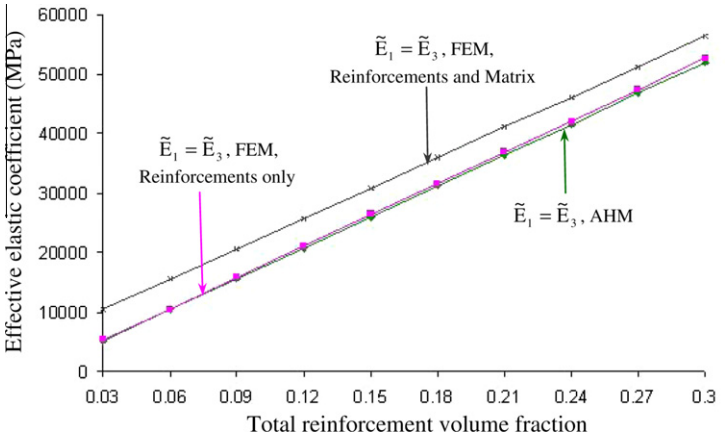

Fig. 13. Variation of the effective stiffness moduli, $\tilde{E}_1$ (or $\tilde{E}_3$), for structure A_1.

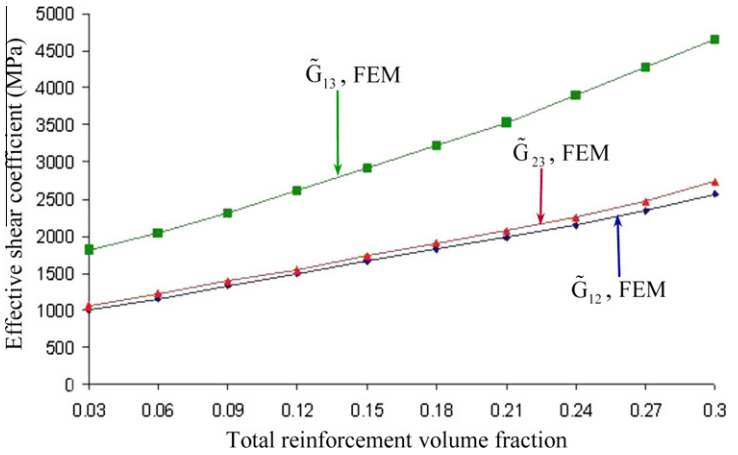

Fig. 14. Variation of the effective shear moduli, $\tilde{G}_{12}$, $\tilde{G}_{23}$ and $\tilde{G}_{13}$, for structure A_1.

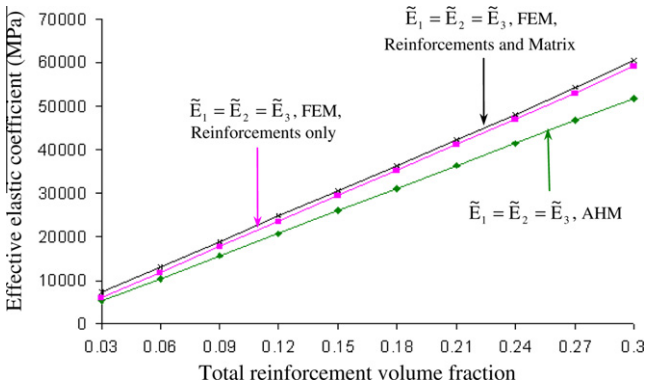

Fig. 15. Variation of the effective stiffness moduli, $\tilde{E}_1 = \tilde{E}_2 = \tilde{E}_3$, for structure A_2.

complex unit cell structures with a larger extend of overlap between reinforcements, this error could be more pronounced. This will be illustrated in subsequent examples.

Finally, Fig. 14 shows the variation of the shear moduli of structure A_1 obtained by the finite element model. These are matrix-dominated properties and thus the asymptotic homogenization model which ignores the contribution of the matrix predicts very low or zero values for these coefficients.

5.2.2. Structure A_2

We now turn our attention to structure A_2shown in the Fig. 9. Fig. 15 shows the variation of the effective elastic moduli vs. the reinforcement volume fraction. Again, three lines are plotted corresponding to the AHM results, the FEM (contribution of reinforcements only) results, and full FEM results (contribution of reinforcements and matrix). Following the discussion in Section 5.2.1, it should be expected that the discrepancy between the AHM results and the FEM results (considering only the reinforcements) is higher for structure A_2 than for structure A_1. This is attributed to a larger volume of overlap between the various reinforcements in the unit cell of structure A_2. Fig. 16 shows a variation of the effective shear moduli of structure A_2 vs. the reinforcement volume fraction.

5.2.3. Structure A_3

The last structure to be considered is structure A_3 shown in the Fig. 10. Following the results in Section 3 (AHM) and Section 4 (FEM) the effective elastic coefficients are determined. Fig. 17 shows the variation of $\tilde{E}_3$ vs. the reinforcement volume fraction.

As with the previous example, the discrepancy between the lower two lines is attributed to the regions of overlap between the different reinforcement families. The difference between the upper two lines is the contribution of the matrix on the effective elastic coefficients.

A comparison of the two modeling techniques readily reveals that the asymptotic homogenization model is appreciably faster in its implementation (without a significant loss of accuracy) and thus is readily amenable to preliminary design of a

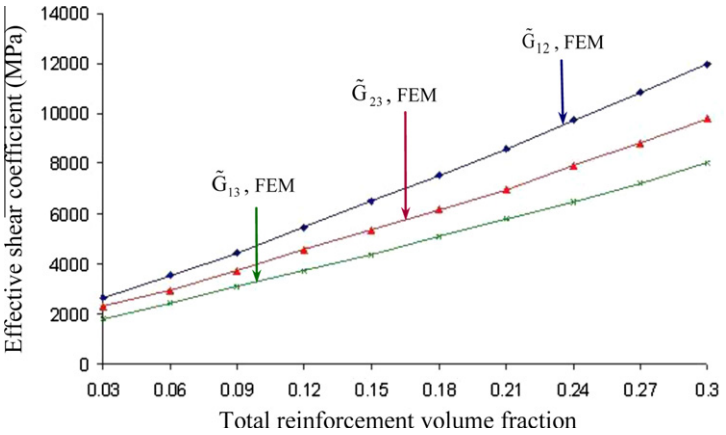

Fig. 16. Variation of the effective shear moduli, $\tilde{G}_{12}$, $\tilde{G}_{23}$ and $\tilde{G}_{13}$, for structure A_2.

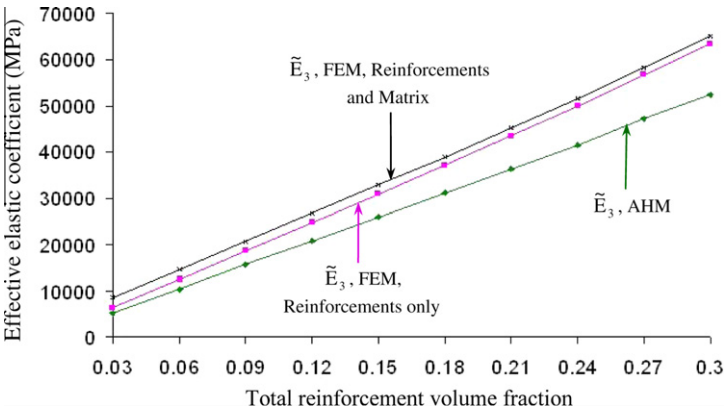

Fig. 17. Variation of $\tilde{E}_3$ for structure A_3.

given 3D grid-reinforced composite structure. The finite element model however, is more accurate and predicts all of the effective elastic coefficients. Thus, the engineer facing a particular design application, could perform a preliminary design (which would normally encompass type, number and spatial orientation of the reinforcements) and then fine tune the final structure (by considering matrix contribution and stress concentration effects) by using the finite element model.

6. Conclusions

A comprehensive micromechanical analysis of 3D periodic composite structures reinforced with a grid of orthotropic reinforcements is undertaken. The general orthotropy of the material of reinforcements is very important from a practical point of view and renders the mathematical problem at hand much more complex.

Modeling is developed on the basis of two different approaches; asymptotic homogenization and finite element techniques. The asymptotic homogenization model decouples the microscopic characteristics of the composite from its macroscopic behavior so that each problem can be handled separately. In doing so, the resultant analysis is significantly simplified. The solution of the microscopic problem leads to the determination of the effective elastic coefficients which are universal in nature and can be used to study a wide variety of boundary value problems.

A finite element model is subsequently developed and used to examine the aforementioned periodic 3D grid-reinforced orthotropic structures. The deformations from the finite element simulations are used to calculate the effective elastic and shear moduli of the structures. The applicability of both models is illustrated by means of various examples of orthotropic grid-reinforced composites. The results of the asymptotic homogenization model are compared to those pertaining to their finite element counterparts and a very good agreement is shown between the two models.

Of particular interest is the fact that the finite element model successfully illustrates the validity of the two key assumptions pertaining to the asymptotic model. In particular, the latter was developed on the assumption that the reinforcements are much stiffer than the surrounding matrix the contribution of which can be ignored. Indeed, the finite element results confirm that the larger the mismatch between the stiffness of the reinforcements and the matrix, the more accurate the asymptotic homogenization model is. Another key assumption of the developed asymptotic homogenization model is that the contribution of the regions of overlap between different reinforcements is small and is not expected to affect significantly the effective elastic coefficients. The finite element results confirm this and indicate that the error that is incurred when ignoring the regions of overlap will only be significant for the cases of structures with more than three different reinforcement families; if the unit cell consists of up to three different reinforcements the associated error is negligibly small.

Given the relative merits of the two modeling techniques, an engineer facing a particular design application, could perform a preliminary design (which would normally encompass type, number and spatial orientation of the reinforcements) and then fine tune the final structure (by considering matrix contribution and stress concentration effects) by using the finite element model.

Acknowledgment

The authors would like to acknowledge the support of the Natural Sciences and Engineering Research Council of Canada (NSERC); the financial assistance of the Cyprus University of Technology; the support of the Brazilian Conselho Nacional de Desenvolvimento Científico (CNPq) and of the National Institute of Science and Technology on Smart Structures for Engineering.

References

Aboudi, J. (1989). Micromechanical analysis of composites by the method of cells. *Applied Mechanics Review, 42*, 193–221.

Aboudi, J. (1996). Micromechanical analysis of composites by the method of cells–update. *Applied Mechanics Review, 49*, 127–139.

Adams, D. F., & Crane, D. A. (1984). Finite element micromechanical analysis of a unidirectional composite including longitudinal shear loading. *Composite Structure, 18*, 1153–1165.

Allen, D. H., & Boyd, J. G. (1993). Convergence rates for computational predictions of stiffness loss in metal matrix composites. In *Composite materials and structures (ASME, New York) AMD 179/AD 37* (pp. 31–45).

Andrianov, I. V., Danishevs'kyy, V. V., & Kalamkarov, A. L. (2006). Asymptotic justification of the three-phase composite model. *Composites Structure, 77*, 395–404.

Bakhvalov, N., & Panasenko, G. (1984). *Homogenization: Averaging processes in periodic media – mathematical problems in the mechanics of composite materials*. Moscow: Nauka.

Bennett, J. G., & Haberman, K. S. (1996). An alternate unified approach to the micromechanical analysis of composite materials, *Journal of Composite Materials, 30*, 1732–1747.

Bensoussan, A., Lions, J. L., & Papanicolaou, G. (1978). *Asymptotic analysis for periodic structures*. Amsterdam: North-Holland.

Berger, H., Kari, S., Gabbert, U., Rodriguez-Ramos, R., Bravo-Castillero, J., Guinovart-Diaz, R., et al (2006). Unit cell models of piezoelectric fiber composites for numerical and analytical calculation of effective properties. *Smart Materials Structure, 15*, 451–458.

Bigelow, C. A. (1993). Thermal residual stresses in a silicon-carbide/titanium [0/90] laminate. *Journal of Composites Technology and Research, 15*, 304–310.

Bystrom, J., Jekabsons, N., & Varna, J. (2000). An evaluation of different models for prediction of elastic properties of woven composites. *Composites Part B, 31*, 7–20.

Caillerie, D. (1984). Thin elastic and periodic plates. *Mathematical Methods in the Applied Science, 6*, 159–191.

Challagulla, K. S., Georgiades, A. V., & Kalamkarov, A. L. (2007). Asymptotic homogenization modeling of thin network structures. *Composite Structures, 79*(3), 432–444.

Challagulla, K. S., Georgiades, A. V., & Kalamkarov, A. L. (2010). Asymptotic homogenization modeling of smart composite generally orthotropic grid-reinforced shells. Part I-Theory. *European Journal of Mechanics A-Solids, 29*, 530–540.

Cioranescu, D., & Donato, P. (1999). *An introduction to homogenization*. Oxford: Oxford University Press.
Daniel, I. M., I, & Ishai, O. (2006). *Engineering mechanics of composite materials*. Oxford: Oxford University Press.
Dasgupta, A., Agarwal, R. K., & Bhandarkar, S. M. (1996). Three-dimensional modeling of woven-fabric composites for effective thermomechanical and thermal properties. *Composites Science and Technology, 56*, 209–223.
Duvaut, G. (1976). Analyse fonctionnelle et méchanique des milieux continues IUTAM. In *Proceedings of the 14th int. cong. on theoretical and applied mechanics (Delft, The Netherlands, 30 August–4 September)* (pp. 119–132).
Georgiades, A. V., Challagulla, K. S., & Kalamkarov, A. L. (2006). Modeling of the thermopiezoelastic behavior of prismatic smart composite structures made of orthotropic materials. *Composites Part B, 37*, 569–582.
Georgiades, A. V., Challagulla, K. S., & Kalamkarov, A. L. (2010). Asymptotic homogenization modeling of smart composite generally orthotropic grid-reinforced shells. Part II-Applications. *European Journal of Mechanics A-Solids, 29*, 541–556.
Georgiades, A. V., & Kalamkarov, A. L. (2004). Asymptotic homogenization models for smart composite plates with rapidly varying thickness: Part II Applications. *International Journal of Multiscale Computer and Engineering, 2*, 149–172.
Guedes, J. M., & Kikuchi, N. (1990). Preprocessing and postprocessing for materials based on the homogenization method with adaptive finite element methods. *Computer Methods in Applied Mechanics and Engineering, 83*, 143–198.
Hassan, E. M., Kalamkarov, A. L., Georgiades, A. V., & Challagulla, K. S. (2009). An asymptotic homogenization model for smart 3D grid-reinforced composite structures with generally orthotropic constituents. *Smart Materials Structure, 18*(7), 075006–075016.
Kalamkarov, A. L. (1992). *Composite and reinforced elements of construction*. New York: Wiley.
Kalamkarov, A. L., Andrianov, I. V., & Danishevs'kyy, V. V. (2009). Asymptotic homogenization of composite materials and structures. *Transactions on ASME, Applied Mechnics Review, 62*(3), 030802-1–030802-20.
Kalamkarov, A. L., Fitzgerald, S., MacDonald, D., & Georgiades, A. V. (1999). On the processing and evaluation of pultruded smart composites. *Composites Part B: Engineering, 30*(2), 167–175.
Kalamkarov, A. L., Fitzgerald, S., MacDonald, D., & Georgiades, A. V. (2000). Mechanical performance of pultruded composites rods with embedded fiber optic sensors. *Journal of Computer Science and Technology, 60*, 1171–1179.
Kalamkarov, A. L., & Georgiades, A. V. (2002a). Modeling of smart composites on account of actuation, thermal conductivity and hygroscopic absorption. *Composites Part B: Engineering, 33*, 141–152.
Kalamkarov, A. L., & Georgiades, A. V. (2002b). Micromechanical modeling of smart composite structures. *Smart Materials and Structures, 11*, 423–434.
Kalamkarov, A. L., & Georgiades, A. V. (2004). Asymptotic homogenization models for smart composite plates with rapidly varying thickness: Part I Theory. *International Journal of Multiscale Computer and Engineering, 2*, 133–148.
Kalamkarov, A. L., Georgiades, A. V., Challagulla, K. S., & Saha, G. C. (2006). Micromechanics of smart composite plates with periodically embedded actuators and rapidly varying thickness. *Journal of Thermoplastic Composite Materials, 19*, 251–276.
Kalamkarov, A. L., & Kolpakov, A. G. (2001). A new asymptotic model for a composite piezoelastic plate. *International Journal of Solids and Structure, 38*, 6027–6044.
Kalamkarov, A. L., Kudryavtsev, B. A., & Parton, V. Z. (1987). The asymptotic method of homogenization in the mechanics of composites with regular structure. *Itogi Nauki i Tekhn. VINITI, 19*, 87–147.
Kohn, R. V., & Vogelius, M. (1984). A new model for thin plates with rapidly varying thickness. *International Journal of Solids Structure, 20*, 333–350.
Kohn, R. V., & Vogelius, M. (1985). A new model for thin plates with rapidly varying thickness, II: A convergence proof. *Quaterly of Applied Mathematics*, 43 1–22.
Lai, W. M., Rubin, D., & Krempl, E. (1993). *Introduction to continuum mechanics*. New York: Pergamon Press.
Li, S. (1999). On the unit cell for micromechanical analysis of fiber-reinforced composites. *Proceedings of Royal Society of London, Series A, 455*, 815–838.
Li, S., & Wongsto, A. (2004). Unit cells for micromechanical analyses of particle-reinforced composites. *Mechanics and Materials, 36*, 543–572.
Maksimov, R. D., Plume, E. Z., & Ponomarev, V. M. (1983). Elastic properties of unidirectionally reinforced hybrid composites. *Mekhanika Komparatist Materials, 1*, 13–19.
Mallick, P. K. (2007). *Fiber-reinforced composites: Materials, manufacturing and design*. Boca Raton: CRC Press.
Michel, J. C., Moulinec, H., & Suquet, P. (1999). Effective properties of composite materials with periodic microstructures: a computational approach. *Computer Methods in Applied Mechanics and Engineering, 172*, 109–143.
Miehe, C., Schroder, J., & Bayreuther, C. (2002). On the homogenization analysis of composite materials based on discretized fluctuation on the micro-structure. *Acta Mechanics, 155*, 1–16.
Mol'kov, V. A., & Pobedrya, B. E. (1985). Effective properties of a unidirectional fiber composite with a periodic structure. *Izvestiya Akademii Nauk SSSR, 2*, 119–130.
Oliveira, J. A., Pinho-da-Cruz, J., & Teixeira-Dias, F. (2009). Asymptotic homogenisation in linear elasticity – Part II: Finite element procedures and multiscale applications. *Computer Materials Science, 45*, 1081–1096.
Paley, M., & Aboudi, J. (1992). Micromechanical analysis of composites by the generalized method of cells. *Mechanics and Materials, 14*, 127–139.
Pettermann, H. E., & Suresh, S. (2000). A comprehensive unit cell model: a study of coupled effects in piezoelectric 1-3 composites. *International Journal of Solids and Structures, 37*, 5447–5464.
Pobedrya, B. E. (1984). *Mechanics of composite materials*. Moscow: Moscow State University.
Pshenichnov, G. I. (1982). *Theory of thin elastic network plates and shells*. Moscow: Nauka.
Reddy, J. N. (2004). *Mechanics of laminated composite plates*. New York: CRC Press.
Saha, G. C., Kalamkarov, A. L., & Georgiades, A. V. (2007a). Effective elastic characteristics of honeycomb sandwich composite shells made of generally orthotropic materials. *Composite Part A, 38*, 1533–1546.
Saha, G. C., Kalamkarov, A. L., & Georgiades, A. V. (2007b). Micromechanical analysis of effective piezoelastic properties of smart composite sandwich shells made of generally orthotropic materials. *Smart Material Structure, 16*, 866–883.
Sanchez-Palencia, E. (1980). *Non-homogeneous media and vibration theory*. *Lecturer Notes Physics* (Vol. 127). Springer-Verlag.
Sluis, O., Schreurs, G., Brekelmans, M., & Meijer, H. (2000). Overall behavior of heterogeneous elastoviscoplastic materials: effect of microstructural modeling. *Mechanics and Materials, 32*, 449–462.
Sun, C. T., & Vaidya, R. S. (1996). Prediction of composite properties from a representative volume element. *Composites Science and Technology, 56*, 171–179.
Suquet, P. M. (1987). Elements of homogenization theory for inelastic solid mechanics. In E. Sanchez-Palencia & A. Zaoui, A. (Eds.), *Homogenization Techniques for Composite Media, Lect. Notes Phys.* (Vol. 272, pp. 193–278).
Tan, P., Tong, L., & Steven, G. P. (1997). Modeling for predicting the mechanical properties of textile composites – A review. *Compsites Part A, 28*, 903–922.
Wang, X. F., Wang, X. W., Zhou, G. M., & Zhou, C. W. (2007). Multi-scale analyses of 3D woven composite based on periodicity boundary conditions. *Journal of Composite Materials, 41*, 1773–1788.
Xia, Z., Zhang, Y., & Ellyin, F. (2003). A unified periodical boundary conditions for representative volume elements of composites and applications. *International Journal of Solids and Structure, 40*, 1907–1921.